



HAL
open science

Cosmology through arc statistics I: sensitivity to $\Omega(m)$ and $\sigma(8)$

Michele Boldrin, Carlo Giocoli, Massimo Meneghetti, Lauro Moscardini,
Giuseppe Tormen, Andrea Biviano

► **To cite this version:**

Michele Boldrin, Carlo Giocoli, Massimo Meneghetti, Lauro Moscardini, Giuseppe Tormen, et al..
Cosmology through arc statistics I: sensitivity to $\Omega(m)$ and $\sigma(8)$. Monthly Notices of the
Royal Astronomical Society, 2016, 457 (3), pp.2738–2748. 10.1093/mnras/stw140 . hal-01434355

HAL Id: hal-01434355

<https://hal.science/hal-01434355>

Submitted on 9 Sep 2021

HAL is a multi-disciplinary open access archive for the deposit and dissemination of scientific research documents, whether they are published or not. The documents may come from teaching and research institutions in France or abroad, or from public or private research centers.

L'archive ouverte pluridisciplinaire **HAL**, est destinée au dépôt et à la diffusion de documents scientifiques de niveau recherche, publiés ou non, émanant des établissements d'enseignement et de recherche français ou étrangers, des laboratoires publics ou privés.



Distributed under a Creative Commons Attribution 4.0 International License

Cosmology through arc statistics I: sensitivity to Ω_m and σ_8

Michele Boldrin,¹★ Carlo Giocoli,^{2,3,4,5} Massimo Meneghetti,^{4,6} Lauro Moscardini,^{2,3,4} Giuseppe Tormen¹ and Andrea Biviano⁷

¹*Dipartimento di Fisica e Astronomia, Università di Padova, vicolo dell'Osservatorio 3, I-35122 Padova, Italy*

²*Dipartimento di Fisica e Astronomia, Alma Mater Studiorum Università di Bologna, viale Bertini Pichat 6/2, I-40127 Bologna, Italy*

³*INFN – Sezione di Bologna, viale Bertini Pichat 6/2, I-40127 Bologna, Italy*

⁴*INAF – Osservatorio Astronomico di Bologna, via Ranzani 1, I-40127 Bologna, Italy*

⁵*CNRS, LAM (Laboratoire d'Astrophysique de Marseille), Aix Marseille Université, UMR 7326, F-13388 Marseille, France*

⁶*Jet Propulsion Laboratory, 4800 Oak Grove Dr., Pasadena, CA 91109, USA*

⁷*INAF – Osservatorio Astronomico di Trieste, via G.B. Tiepolo 11, I-34143 Trieste, Italy*

Accepted 2016 January 14. Received 2016 January 14; in original form 2015 May 14

ABSTRACT

The next generation of large sky photometric surveys will finally be able to use arc statistics as a cosmological probe. Here, we present the first of a series of papers on this topic. In particular, we study how arc counts are sensitive to the variation of two cosmological parameters: the (total) matter density parameter, Ω_m , and the normalization of the primordial power spectrum, expressed in terms of σ_8 . Both these parameters influence the abundances of collapsed structures and their internal structure. We compute the expected number of gravitational arcs with various length-to-width ratios in mock light cones, by varying these cosmological parameters in the ranges $0.1 \leq \Omega_m \leq 0.5$ and $0.6 \leq \sigma_8 \leq 1$. We find that the arc counts dependence on Ω_m and σ_8 is similar, but not identical, to that of the halo counts. We investigate how the precision of the constraints on the cosmological parameters based on arc counts depend on the survey area. We find that the constraining power of arc statistics degrades critically only for surveys covering an area smaller than 10 per cent of the whole sky. Finally, we consider the case in which the search for arcs is done only in frames where galaxy clusters have been previously identified. Adopting the selection function for galaxy clusters expected to be detected from photometric data in future wide surveys, we find that less than 10 per cent of the arcs will be missed, with only a small degradation of the corresponding cosmological constraints.

Key words: gravitational lensing: strong – galaxies: clusters: general – cosmology: theory.

1 INTRODUCTION

The importance of galaxy clusters in cosmology is well known (for a review, see Allen, Evrard & Mantz 2011, and references therein). Being the most massive bound systems in the Universe, they trace the latest stage of structure formation. Their abundance and mass as a function of redshift are thus highly indicative of how the growth of the cosmic density fluctuations occurs and can thus be used to constrain the matter content, the initial power spectrum normalization and the expansion history of the Universe (Eke et al. 1998; Borgani et al. 2001; Reiprich & Böhringer 2002; Allen et al. 2003; Schuecker et al. 2003; Henry 2004; Vikhlinin et al. 2009; Mantz et al. 2010; Rozo et al. 2010; Sehgal & et al. 2011; Benson et al. 2013; Mantz et al. 2014; Planck Collaboration XX 2014b).

Moreover, galaxy clusters are essential cosmic laboratories where the complex interaction between baryons and dark matter can be

studied in detail, in particular during merger events (Clowe et al. 2006; Merten et al. 2011).

Being the most massive structures in the Universe, galaxy clusters are also the most powerful gravitational lenses (Narayan & Bartelmann 1999; Bartelmann & Schneider 2001; Kneib & Natarajan 2011). In particular, they are responsible for highly non-linear lensing effects taking place in their densest regions, i.e. in their cores. In this so-called strong lensing regime, the images of background galaxies are heavily distorted, often leading to the appearance of gravitational arcs with large length-to-width ratios (see Kneib & Natarajan 2011; Meneghetti et al. 2013, and references therein).

The efficiency of galaxy clusters to produce arcs with a given ratio between their length l and width w is quantified by means of their strong lensing cross-section $\sigma_{l/w}$. This is defined as the area on the source plane where the source has to be located in order to form an arc with such an l/w ratio. To have a large strong lensing cross-section, the projected mass distribution of the lens must be exceptionally dense on the plane of the sky, also called ‘lens plane’. Sometimes, this can be the result of projection effects (haloes

* E-mail: michele.boldrin@studenti.unipd.it

elongated along the line of sight, superposition of multiple structures at different redshifts, etc.), but, generally speaking, gravitational arcs trace the highest peaks in the cosmological density field. Bartelmann et al. (1998) first pointed out that counting gravitational arcs may be a competitive method to constrain cosmological parameters (see e.g. Fedeli et al. 2006; Meneghetti et al. 2013).

Unfortunately, strong lensing events such as gravitational arcs are rare. Given the relatively low number of arcs discovered so far and the high inhomogeneity of cluster optical surveys, the application of arc statistics in cosmology has been attempted mainly with the goal of possibly falsifying the standard cosmological model (the so-called concordance Λ CDM) rather than actually constraining cosmological parameters. For about 15 years, scientists have debated on the existence or non-existence of a tension between the observed number of arcs and the predictions derived in the framework of the cosmological model favoured by observational data (see Meneghetti et al. 2013, and references therein). Undoubtedly, arc statistics suffered so far from the lack of suitable large observational data sets for a reliable comparison to theoretical predictions. The situation is likely to change radically in the near future, thanks to the advent of large optical surveys, covering areas in the range from several thousands of square degrees (de Jong et al. 2013; The Dark Energy Survey Collaboration 2005), to (almost) the full sky (Karoji 2009; LSST Science Collaboration et al. 2009; Laureijs et al. 2011; Spigel et al. 2013).

In Boldrin et al. (2012), we forecasted the number of gravitational arcs visible in the future wide-field survey to be performed by the ESA *Euclid* mission (Laureijs et al. 2011). A further step is the analysis of the sensitivity of arc statistics on cosmological parameters. In particular in this work, we focus on the dependence of arc statistics on the (total) matter density parameter Ω_m and on the normalization of the primordial power spectrum, expressed in terms of σ_8 . More precisely, we investigate the region of the parameter space defined by $\Omega_m = [0.1-0.5]$, and $\sigma_8 = [0.6-1.0]$. We sample the parameters at intervals $\Delta\Omega_m = 0.1$ and $\Delta\sigma_8 = 0.1$, thus investigating a total of 25 different cosmological models, always making the assumption of a flat Universe ($\Omega_m + \Omega_\Lambda = 1$). To help a direct comparison with the results of Boldrin et al. (2012), here we assume a reference cosmology defined by the parameters ($\Omega_m = 0.272$, $\sigma_8 = 0.809$) with present Hubble parameter $H_0 = 70.4 \text{ km s}^{-1} \text{ Mpc}^{-1}$, in agreement with the *Wilkinson Microwave Anisotropy Probe 7* (WMAP7) results (Komatsu et al. 2011). However, we will discuss also the results obtained with the assumption of the parameters recently derived by Planck Collaboration XVI (2014a).

The paper is organized as follows. In Section 2, we briefly describe the method adopted to compute the number of arcs and to build the mock catalogues. In Section 3, we present our main results, i.e. the total number of arcs and their redshift distribution as a function of Ω_m and σ_8 . Section 4 is devoted to a discussion of the origin of the cosmological influence on arc statistics; we also consider how the results can change when including the effects of possible systematics. In Section 5, we discuss the agreement between the predictions obtained with our methodology and the arc counts in real surveys, using the recent results of Xu et al. (2016) based on the Cluster Lensing And Supernova survey with Hubble (CLASH) survey. Finally, in Section 6, we summarize and draw our conclusions.

2 METHOD

In this section, we summarize the steps undertaken for calculating the number of arcs produced by a population of strong lenses.

2.1 Generation of lenses with MOKA

In the attempt of properly modelling all the relevant structural properties of the lenses in our calculations of $\sigma_{l/w}$, we make use of the pseudo-analytic code MOKA (Giocoli et al. 2012a,b). This code allows us to generate mock cluster-size gravitational lenses in any desired cold dark matter (CDM) scenario, including features like triaxiality and projection effects, scatter in concentration, substructures, and the presence of a brightest central galaxy, including the effects that its growth produces adiabatic contraction on the cluster dark matter halo profile. As discussed in several earlier works based on fully numerical simulations (see e.g. Meneghetti, Bartelmann & Moscardini 2003; Torri et al. 2004; Meneghetti et al. 2007), all these features play an important role for determining the cluster ability to produce giant arcs. The most important novelty of our work mainly lies on the adoption of very realistic simulated strong lenses, as the MOKA code allows to do.

More in detail, to generate the mock lenses, we use the following prescriptions:

- (i) the host halo mass density profile is described by the Navarro, Frenk and White radial function (Navarro, Frenk & White 1996);
- (ii) the dark matter halo concentration is derived from the mass-concentration relation proposed by Zhao et al. (2003), assuming lognormal scatter of $\sigma_{\ln c} = 0.25$;
- (iii) the lens halo is triaxial and the axis ratios are generated assuming the triaxial distributions derived by Jing & Suto (2002);
- (iv) the spatial orientation is randomly chosen;
- (v) the substructure abundance follows the subhalo mass function derived by Giocoli, Tormen & van den Bosch (2008);
- (vi) the substructure radial distribution follows that proposed by Gao et al. (2004);
- (vii) the substructures are modelled as Single Isothermal Spheres (Metcalf & Madau 2001);
- (viii) the mass density profile of the Brightest Cluster Galaxy (BCG) resembles the Hernquist's profile (Hernquist 1990).

The main outcome of the MOKA code is the deflection angle map of each mock halo. From the latter, we obtain $\sigma_{l/w}$ for sources at $z_s = 2$ via ray-tracing technique. For simplicity, we consider only isolated lenses, avoiding the cases of merging haloes, even though some studies revealed the importance these events have on the amplitude of the strong lensing signal (see e.g. Torri et al. 2004). Furthermore, another source of enhancement of the signal is given by the large-scale structure present along the line of sight, which boosts the lens projected mass on the source plane. Since beyond purpose of this paper, we postpone detailed studies of those two aspects to a future work.

2.2 Number of giant arcs

We trace light rays through a uniform grid on the lens plane towards the source plane, accounting for the position-dependent deflections. The source plane is populated with elliptical sources distributed on a regular grid. Their lensed shapes are recovered by collecting the light rays hitting them. The lengths and widths of the resulting gravitational arcs are measured using the method described in several earlier papers (see e.g. Meneghetti et al. 2003). As in Boldrin et al. (2012), the source population has random ellipticity and an apparent size depending on the redshift (see Boldrin et al. 2012, fig. 3). To properly sample the region of the source plane, where sources are lensed as giant arcs, we iteratively increase the resolution of source grid near the lens caustics. Each source is then representative of

an area on the source plane defined by the local resolution of the source grid. Using this area as weight, we compute $\sigma_{l/w}$, defined as the area on the source plane within which a source has to be located for being lensed as a giant arc with a given l/w (Meneghetti et al. 2008).

The number of arcs with length-to-width ratio larger than l/w , produced by a lens of mass M at redshift z_l , can be computed solving the following relation:

$$N_{l/w}(M, z_l) = \sigma_{l/w}(2) \int_{z_l}^{z_{s,\max}} dz_s f_\sigma(z_l, z_s) n(z_s, S), \quad (1)$$

where $\sigma_{l/w}(2) \equiv \sigma_{l/w}(M, z_l, z_s = 2)$ is the strong lensing cross-section for giant arcs for sources at redshift $z_s = 2$, and $f_\sigma \equiv \frac{\sigma_{l/w}(z_s)}{\sigma_{l/w}(z_s=2)}$ accounts for the scaling of $\sigma_{l/w}$ with z_s . In order to minimize the computational time, we recover the scaling function f_σ computing $\sigma_{l/w}(z_s)$ of a lens subsample, adopting different values of z_s (see for more details Boldrin et al. 2012).

A crucial ingredient is the redshift distribution of the sources exceeding a given surface brightness S , $n(z_s, S)$. We derive it by simulating an observation of the galaxies in the *Hubble-Ultra-Deep-Field (HUDF)* using the SKYLENS code (Meneghetti et al. 2008), to a depth which is reasonable for a future wide-field survey from space. As a reference, we consider the *Euclid* wide survey, which is expected to reach an average limiting magnitude $m_{\text{riz}} = 24.5$ (Laureijs et al. 2011). Adopting typical *Euclid*-like exposure times and background levels, we estimate the surface brightness limits corresponding to 1σ and 3σ above the mean background level, and use the simulated observations of the *HUDF* to measure $n(z_s, S)$. Using a subset of MOKA lenses to simulate observations of gravitational arcs, we find that we can safely neglect from the giant arc counts sources above $z_{s,\max} = 6$.

For each combination of cosmological parameters, we produce a catalogue of cluster-sized lenses with different masses and redshifts. We define 100 mass bins which are uniformly spaced in logarithm between 10^{13} and $10^{16} h^{-1} M_\odot$ and eight redshift bins, having $\Delta z = 0.03$ and centred at redshifts 0.21, 0.36, 0.54, 0.6, 0.84, 1.02, 1.14 and 1.26. The choice of such redshift bins is optimized for the expected redshift distribution of the lenses producing giant arcs, which we derived in Boldrin et al. (2012) for a *Euclid*-like survey. For each combination of redshift and mass, we use MOKA to generate 100 haloes with different structural properties and measure their $\sigma_{l/w}$, from which we can derive the number of giant arcs they produce, as discussed above.

The catalogue of lenses is then used to generate 128 realizations of lens distributions (light-cones). In each light-cone, which subtends an area of $15\,000 \text{ deg}^2$, we calculate the number of lenses of mass M and redshift z_l according to the Sheth & Tormen (1999) mass function, and estimate the total number of arcs by summing up the contributions from each individual lens. Finally, we combine the different light-cones to measure the median number of arcs per square degree and the relative scatter as a function of the considered cosmological parameters.

3 RESULTS

3.1 Number of arcs as a function of redshift

We begin by discussing how the arc counts change as a function of cosmology in different redshift bins. In Fig. 1, we show the number of arcs, normalized to the reference *WMAP7* cosmology, as function of Ω_m . The different panels refer to the eight redshifts where the calculations were performed. Different colours and line

styles are used to display the results for several values of σ_8 : solid blue, dotted cyan, dashed green, long-dashed brown and dot-dashed dark orange lines refer to $\sigma_8 = 0.6, 0.7, 0.8, 0.9$ and 1 , respectively. Long-dashed black horizontal lines correspond to unity, i.e. to the reference cosmology. The lack of a blue solid line in the last panel is due to the inefficiency of clusters at $z_l = 1.26$ to produce giant arcs in the cosmology with $\sigma_8 = 0.6$. As expected, at all redshifts, the arc counts grow as a function of Ω_m and as a function of σ_8 , indicating that the abundance of giant gravitational arcs is higher in cosmological models with more matter and higher normalization of the power spectrum of the primordial density fluctuations.

We also notice that the change of arc counts as a function of cosmology depends on the lens redshift. The dependence on Ω_m is stronger at lower redshift, and flattens off as z_l increases. On the contrary, it appears that the value of σ_8 affects the results more significantly at high redshift.

While the results in Fig. 1 refer to arcs with $l/w \geq 10$ and sources above the 1σ background level, the trends remain similar for other l/w ratios and detection limits.

3.2 The total number of arcs

From the distributions obtained from the 128 different light-cone realizations, we measure the median number of arcs per square degree expected in each cosmological model. This has been done by performing a spline interpolation through the above-mentioned eight redshifts up to a maximum lens redshift of $z_l = 1.5$.

In the reference *WMAP7* cosmology, the expected number densities of arcs per square degree with $l/w \geq 5, 7.5$ and 10 are $0.594 \pm 0.016, 0.194 \pm 0.006$ and 0.085 ± 0.003 , respectively. These are in excellent agreement with our estimates reported in Boldrin et al. (2012), although these were obtained using a larger number of redshift bins and avoiding the interpolation.

In Fig. 2, we show the median arc number counts per square degree as a function of Ω_m . We also show how the counts vary by changing the value of σ_8 , using the same colour and line styles used in Fig. 1. From top to bottom, we show the results for $l/w \geq 5, 7.5$ and 10 , respectively. The left-hand and the right-hand panels refer to detections at 1σ and 3σ above the level of the background. Obviously, the results show the same dependence on Ω_m and σ_8 reported in Fig. 1.

We also see that the ratios between counts of arcs with different l/w depend on the cosmological parameters. As shown in Fig. 3, for low Ω_m , the abundance of arcs with $l/w \geq 5$ or $l/w \geq 7.5$, relative to that of arcs with $l/w \geq 10$, is higher, indicating that haloes in these cosmological models have smaller critical lines and are thus less efficient at producing large distortions. The ratios also depend on σ_8 ; in cosmologies with higher σ_8 haloes are able to produce a higher abundance of arcs with large l/w . The results (here shown only for sources 1σ above the mean background level) are insensitive to the assumed detection limit. Therefore, in the following discussion we will show the results only for arcs detectable at the 1σ level. We will also focus on arcs with $l/w \geq 10$.

The upper panel in Fig. 4 shows the difference in the arc counts relative to the reference *WMAP7* cosmology in the Ω_m - σ_8 plane. Within the ranges explored in this work, we may find differences of up to one order of magnitude for the predicted arc counts between cosmological models. We also notice that the cosmological parameters Ω_m and σ_8 are degenerate with respect to the arc counts. Indeed, the same number of arcs is expected in cosmologies whose combination of Ω_m and σ_8 lays in a banana-like region extending from the upper left to the bottom right corner of the plane. The origin of this

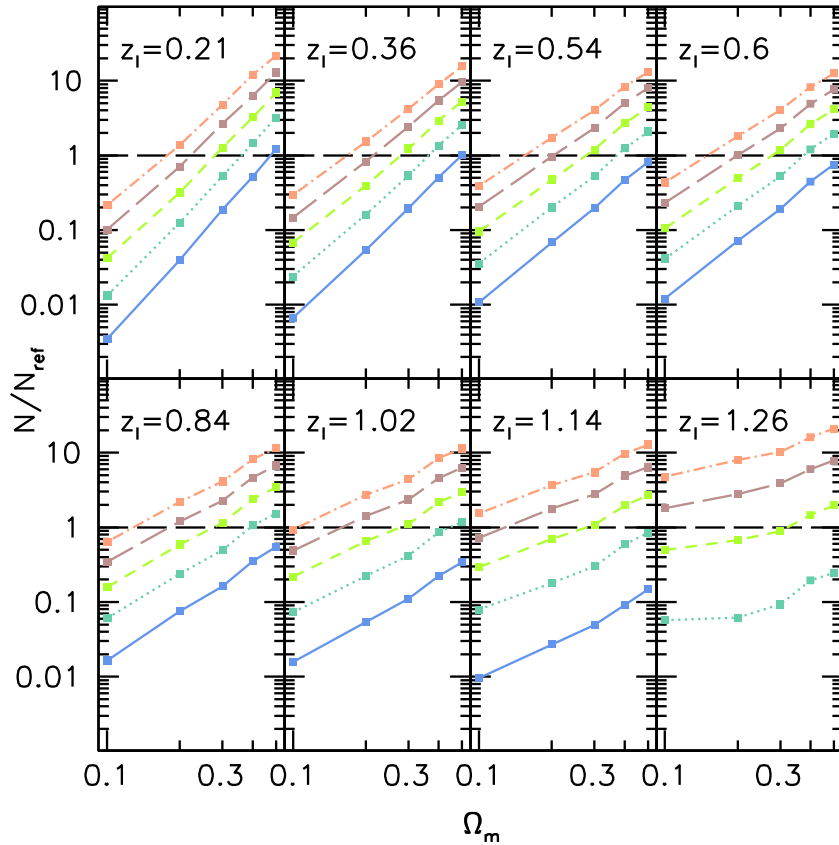


Figure 1. Number of arcs (normalized to the reference *WMAP7* cosmology) as function of Ω_m and for different values of σ_8 . Different panels refer to different redshift bins between $z = 0.21$ and $z = 1.26$, as labelled. The reported counts represent the median of 128 different light-cone realizations for each combination of the cosmological parameters. Solid blue, dotted cyan, dashed green, long-dashed brown and dot-dashed dark orange lines indicate the results for $\sigma_8 = 0.6, 0.7, 0.8, 0.9$ and 1 , respectively. The results refer to arcs with $l/w \geq 10$ and sources 1σ above the mean background noise level.

degeneracy will be better discussed in Section 4.1. Interestingly, a *Planck*-like cosmology with $\Omega_m = 0.3086$ and $\sigma_8 = 0.8288$ (Planck Collaboration XVI 2014a) produces 54 per cent more arcs than the reference *WMAP7* cosmology.

We find that in the case of the reference *WMAP7* model, the equation describing the degeneracy curve between the cosmological parameters has the following form:

$$\Omega_m = A\sigma_8^2 + B\sigma_8 + C, \quad (2)$$

where $A = 1.771$, $B = -3.952$ and $C = 2.31$. Such function is given by the white line in the upper panel of Fig. 4.

In the attempt to quantify the uncertainty in the arc counts, we define the 1σ uncertainty on the number counts as $\sigma \equiv (\sigma_{\text{CV}}^2 + \sigma_p^2)^{1/2}$, where σ_{CV} is the cosmic variance, which is estimated from the 16th and 84th percentiles of the distributions derived from the 128 light-cone realizations of each tested cosmological model. The other term appearing in the equation, $\sigma_p \equiv \sqrt{N}$, is the associated Poisson noise on the number counts.

In the bottom panel of Fig. 4, we perform an error analysis showing the levels corresponding to 1σ , 3σ and 5σ deviations (from dark to light colours) from the *WMAP7* and the *Planck* cosmologies in the Ω_m - σ_8 plane. The results were obtained assuming a survey covering $15\,000 \text{ deg}^2$ of the sky to the depth expected for the *Euclid* mission. It is interesting to notice that a survey with the *Euclid* characteristics will be able to distinguish these two cosmological models at more than 5σ level.

4 DISCUSSION

4.1 Influence of the cosmological parameters on arc statistics

In this section, we will discuss in more detail some aspects of the influence of Ω_m and σ_8 on arc statistics. In general, the cosmological parameters play an important role in arc statistics through the lens mass function and their strong lensing cross-section, the latter depending on the geometry of the Universe and on the structural properties of the lens halo.

In particular, the number of arcs is directly related to the number of lenses able to produce arcs. Following Meneghetti et al. (2010, 2011), this can be estimated including in the mass function describing the lens distribution a sharp cut at the minimum mass corresponding to the smallest systems in which we expect to find critical lines for sources at $z_s = 2$. The shape of the adopted selection function as a function of redshift is shown by the black curve in Fig. 5 (see also Boldrin et al. 2012).

In Fig. 6, we present the number density (given per square degree) of the lenses as a function of redshift. In each panel, we keep fixed Ω_m as labelled and we vary the value for σ_8 , using the colour code indicated on the bottom right. To facilitate the comparison, the lens number density in the reference *WMAP7* cosmology is shown in black in all panels. From the figure, the strong effect of the different matter density on the lens abundances and the anticipated structure formation originated by a higher power spectrum normalization are clear.

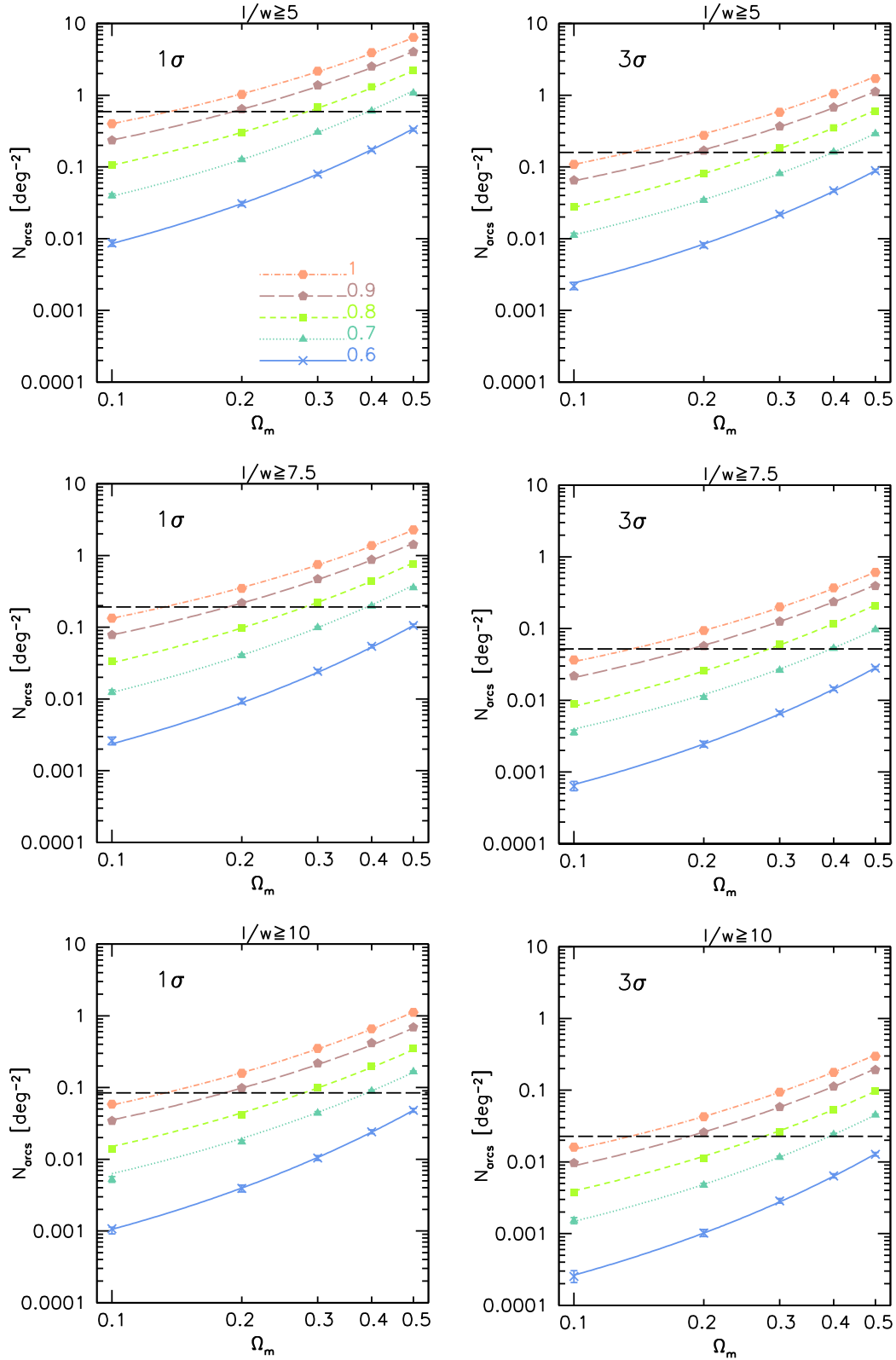


Figure 2. Number density of arcs as a function of Ω_m for different values of σ_8 . The right and left columns refer to sources detectable at 1σ and 3σ above the mean background noise level, respectively. From top to bottom, the different panels show the results for three choices of minimum l/w , namely 5, 7.5 and 10. Line and colour styles are as in Fig. 1. In each panel, the horizontal dashed line shows the counts in the considered reference model.

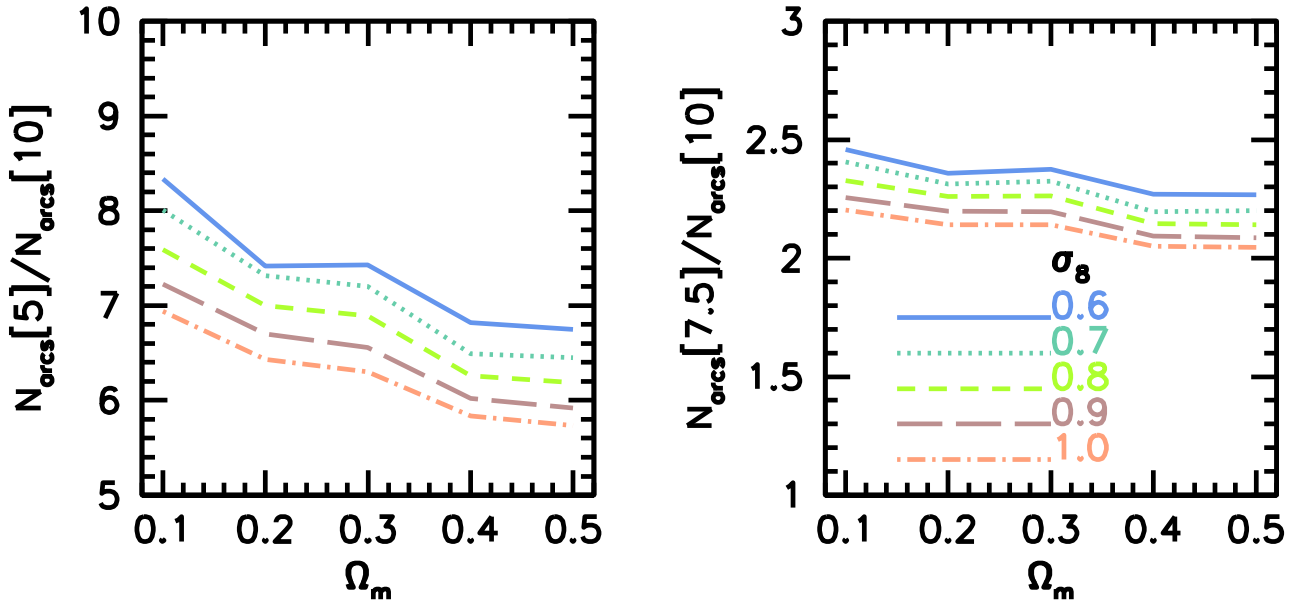


Figure 3. The abundances of arcs with $l/w \geq 5$ (left-hand panel) and $l/w \geq 7.5$ (right-hand panel) relative to the abundances of arcs with $l/w \geq 10$ as a function of Ω_m . Line and colour styles are as in Fig. 1. The results refer to arcs detectable at 1σ above the mean background level.

In Fig. 7, adopting the same colour code as in the upper panel of Fig. 4, we show the difference in the lens counts relative to the reference *WMAP7* cosmology in the Ω_m – σ_8 plane. The white solid curve in the figure represents the degeneracy between Ω_m and σ_8 for the halo counts, for which we find the following relation:

$$\sigma_8(\Omega_m/0.272)^{0.304} = 0.809. \quad (3)$$

Even if with some differences, this curve is close to the relation (shown by the white crosses) representing the degeneracy we found in the Ω_m – σ_8 plane for the arc counts (see also Fig. 4): this is clearly due to the fact that the most important ingredient for arc statistics is the lens mass function. However, if one compares the amplitude of the count variation by looking at the width of the coloured strips, it is evident that the arc density is more sensitive to the cosmological parameters than the simple halo density: consequently, a wide survey of gravitational arcs could potentially give significant constraints.

The larger sensitivity of arc statistics is due to the cosmological dependence of the other main ingredients, such as the angular diameter distances of lenses and sources and the lens structural properties. We know that the first condition for an axially symmetric lens to act like a strong lens is that in some points \mathbf{x} on the lens plane the condition

$$\kappa(\mathbf{x}) > 1 \quad (4)$$

occurs, where $\kappa \equiv \Sigma(\mathbf{x})/\Sigma_{\text{cr}}$ is the so-called convergence, $\Sigma(\mathbf{x})$ is the lens projected mass density and

$$\Sigma_{\text{cr}} \equiv \frac{c^2}{4\pi G} D_{\text{lens}}^{-1} \quad (5)$$

represents the critical value of the two-dimensional mass density in order to have strong lensing effects. The quantity D_{lens} is the so-called *lensing distance*, defined as

$$D_{\text{lens}} \equiv \frac{D_{\text{LS}} D_{\text{L}}}{D_{\text{S}}}, \quad (6)$$

where D_{S} , D_{L} and D_{LS} are the angular diameter distances of the source, of the lens and between source and lens, respectively. Although for elliptical lenses we have to add the effect of shear to the condition (4), we can infer, to first approximation, what are the system configurations which are more efficient in producing strong lensing features by investigating how D_{lens} changes in the different cosmological models, once the lens properties and the source redshifts are kept fixed. We remind the reader that D_{lens} contains the full dependence on the geometry of the system and does not depend on σ_8 , but only on Ω_m . We fix the source position at redshift $z_s = 2$ and we study $D_{\text{lens}}(z_l)$, that is we keep fixed the length of the lensing system and we move the lens from the observer towards the source plane. The results are shown in Fig. 8: we see that increasing the value of Ω_m , the strong lensing efficiency reaches its maximum at lower lens redshifts. In particular, the peak around which the production of gravitational arcs is expected to be boosted shifts from $z \approx 0.6$ to $z \approx 0.4$ when the value of Ω_m is increased from 0.1 to 0.5.

The effect of the anticipation of structure formation due to a higher value of σ_8 (Giocoli et al. 2007, 2012b) has consequences on several halo structural properties that may influence the size of $\sigma_{l/w}$. Considering the concentration parameter, at fixed σ_8 , large Ω_m values lead to larger concentrations because the structures form and grow in denser environments. At the same time, keeping fixed the value of Ω_m , in cosmologies with high σ_8 the concentration increases because of both the higher contrast between primordial perturbations and background, and the anticipated formation time (Neto et al. 2007; Macciò, Dutton & van den Bosch 2008; Giocoli et al. 2012b).

Halo triaxiality is also an important feature that depends on cosmological parameters (Despali, Giocoli & Tormen 2014; Bonamigo et al. 2015). In particular, the level of sphericity of a halo, which is directly related to the ratio between its minor and major semi-axes a/c , is an increasing function of σ_8 and a decreasing function of Ω_m . As an example, if we consider haloes with a mass equal to $7.5 \times 10^{14} h^{-1} M_{\odot}$ at redshift $z = 0.54$ in a cosmological model with $\Omega_m = 0.3$, the median ratio among 128 realizations varies from $a/c = 0.353^{+0.049}_{-0.056}$ in a model with $\sigma_8 = 0.6$, to $a/c = 0.417^{+0.057}_{-0.066}$ in

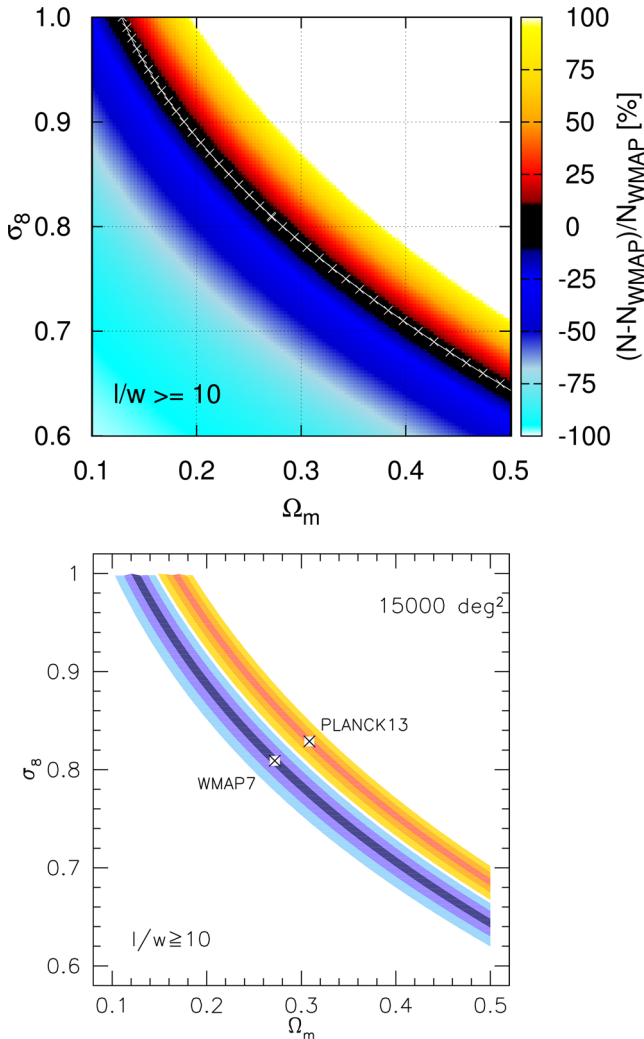


Figure 4. Upper panel: difference in the arc counts with respect to the reference WMAP7 cosmology in the Ω_m - σ_8 plane. The results are shown for arcs with $l/w \geq 10$ detectable at 1σ above the background level. The white crosses represent the cosmological models having the same arc counts as the reference WMAP7 model [relation (2)]. Bottom panel: levels corresponding to 1σ , 3σ and 5σ deviations (from dark to light colours) from the WMAP7 (blue) and the Planck (yellow) cosmologies in the Ω_m - σ_8 plane, assuming a 15000 deg^2 survey to the expected depth of the *Euclid* wide survey. The crosses indicate the position of the two reference models.

a model with $\sigma_8 = 1.0$. The quoted uncertainties correspond to 1σ errors. On the other hand, if we fix $\sigma_8 = 0.8$, the ratio changes from $a/c = 0.419^{+0.058}_{-0.066}$ in a model with $\Omega_m = 0.1$, to $a/c = 0.388^{+0.053}_{-0.061}$ in a model with $\Omega_m = 0.5$.

4.2 Effects of completeness and cluster selection function

In the following subsections, we will discuss how our results change when we take into account the lack of completeness and when we introduce a realistic photometric galaxy cluster selection function.

4.2.1 The effect of sample completeness and survey area

Let us consider here the case in which a fraction of arcs are missed, independently of the properties of the lens configurations (l/w , z_l , z_s). This may happen because some arcs may escape detection

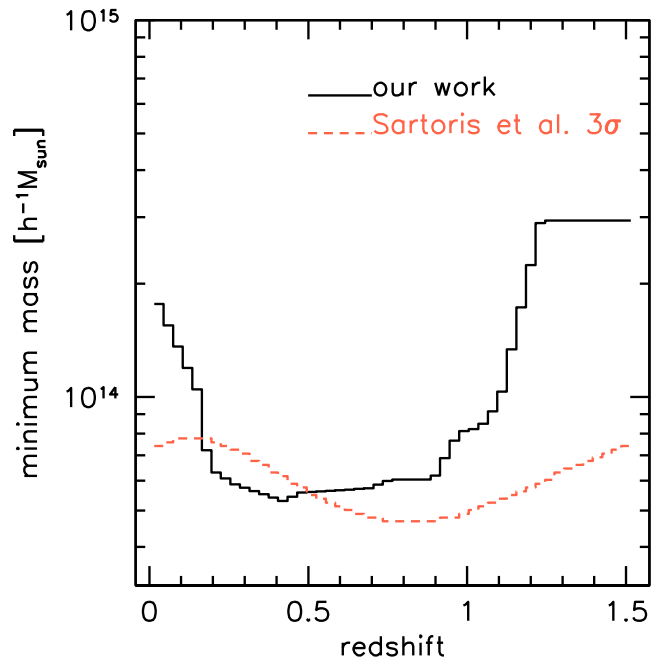


Figure 5. The strong lensing selection function (black solid curve), i.e. the minimum galaxy cluster mass expected to produce critical lines for sources located at $z_s = 2$ (Meneghetti et al. 2010; Boldrin et al. 2012). For comparison, the red dashed curve represents the minimum mass of galaxy clusters which are expected to be detected above three times the rms of the field galaxy counts in the *Euclid* photometric survey (Sartoris B. et al. 2015).

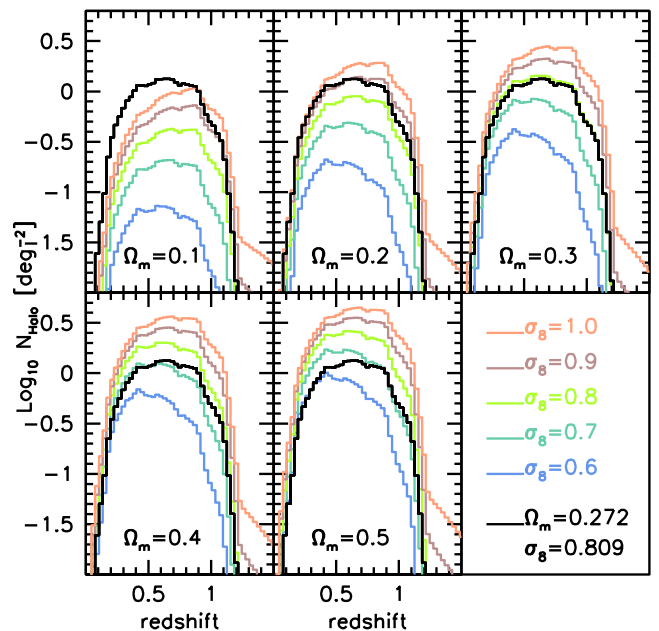


Figure 6. Number density of expected strong lenses as a function of redshift, for cosmologies with different Ω_m and σ_8 . Plots from left to right and from up to bottom refer to increasing values of Ω_m . Different colours represent counts for various values of σ_8 , as labelled on the bottom right. The black line shown in all panels represents the results for the reference WMAP7 model.

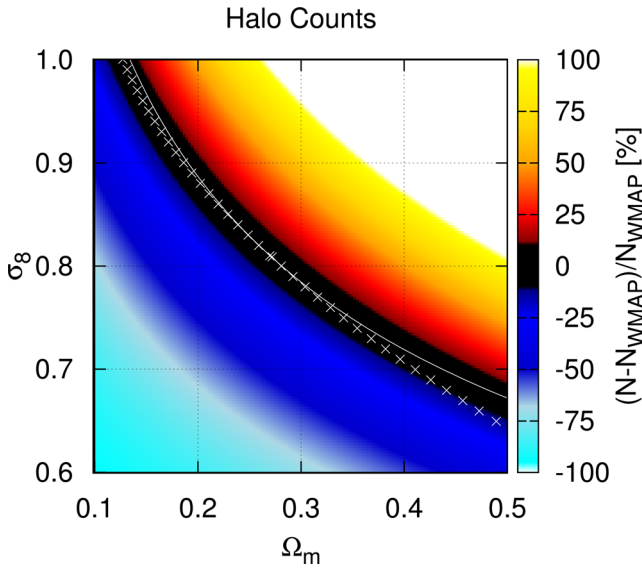


Figure 7. Relative difference of halo counts on the σ_8 - Ω_m plane with respect to the reference *WMAP7* model. The white crosses represent the degeneration curve relative to the arc counts, while the white solid line refers to the degeneration curve for halo counts.

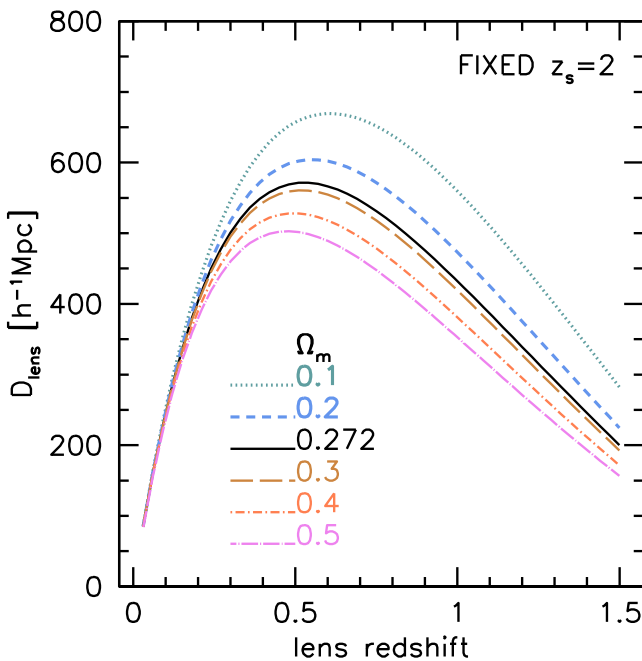


Figure 8. Lensing distance for different values of Ω_m . Sources are kept fixed at redshift $z_s = 2$.

for some particular configurations of the light distribution within the cluster, or when the separation between cluster and foreground galaxies is made difficult by the lack of precise colour information. The total arc counts may also diminish because we are performing our search in a reduced effective area, smaller than the one of the running survey. In this situation, losing 10 per cent of the counts is equivalent to observe a portion of sky 10 per cent smaller than the original survey. The obvious consequence of a reduction of the number of observed arcs is that the Poissonian uncertainty grows and can start to dominate with respect to the cosmic variance, when accounting for the total error budget. To quantify this effect, in

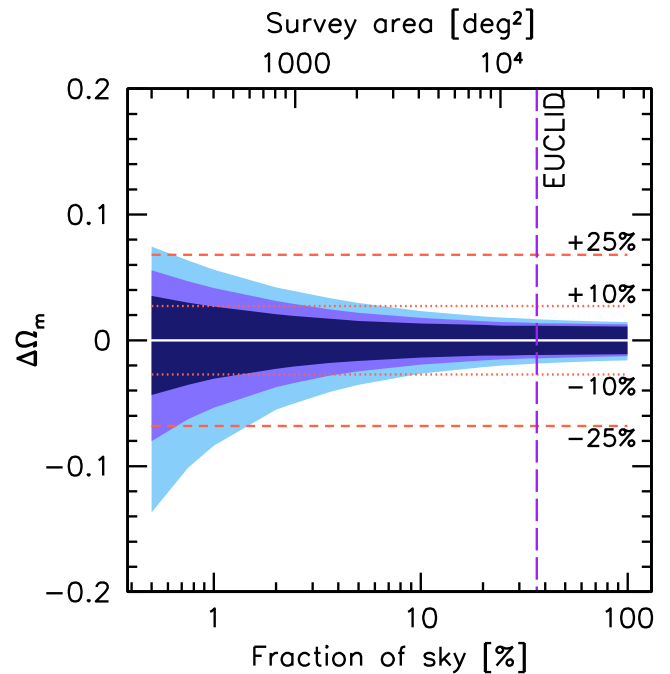


Figure 9. The amplitude of the 3σ error bar on Ω_m as a function of the survey area. The vertical dashed line shows the size of the future *Euclid* wide survey. The red horizontal dotted and dashed lines represent a variation of Ω_m corresponding to ± 10 per cent and ± 25 per cent, respectively.

Fig. 9 we show, as a function of the fraction of the sky covered by the arc search, the variation of the 3σ error bar on the parameter Ω_m , when the value of σ_8 is a priori fixed to its reference value ($\sigma_8 = 0.809$), as it may happen if independently measured from other cosmological probes. Dark, medium and light blue regions refer to the cases of arcs with $l/w \geq 5, 7.5$ and 10 , respectively, while the horizontal dotted (dashed) lines indicate an accuracy of 10 (25) per cent on Ω_m . From the figure, it is clear that arcs with $l/w \geq 5$, being more numerous, give stronger constraints and are less affected by possible incompleteness problems. However, there is a difficulty when dealing with them because they can look like simple edge-on galaxies. For this reason the loss and misidentification of arcs are expected to depend on l/w , being stronger for low- l/w ratios. From this point of view, Fig. 9 is quite encouraging: if the survey area is sufficiently wide (larger than 10 per cent of the whole sky), or equivalently if the arc finders are sufficiently efficient, the error budget is dominated by cosmic variance and there is not a significant difference in the constraining power between using arcs with $l/w \geq 5$ or with $l/w \geq 10$. We remind that the SDSS (York et al. 2000) has an area of about $10\,000 \text{ deg}^2$, while the *Euclid* wide survey is expected to cover $15\,000 \text{ deg}^2$ (Laureijs et al. 2011).

4.2.2 The effect of the cluster selection function

Due to the high computational cost of the algorithms for arc detection, a possible strategy in future wide surveys is to run these codes only on small-size frames where galaxy clusters have been previously identified. Obviously, this originates a reduction of the effective number of arcs, which is strongly dependent on the specific cluster selection function of the survey.

As a worked example, here we consider again the future ESA *Euclid* mission. Given the amount and quality of its data covering an area of $15\,000 \text{ deg}^2$, there will be at least three main ways to identify

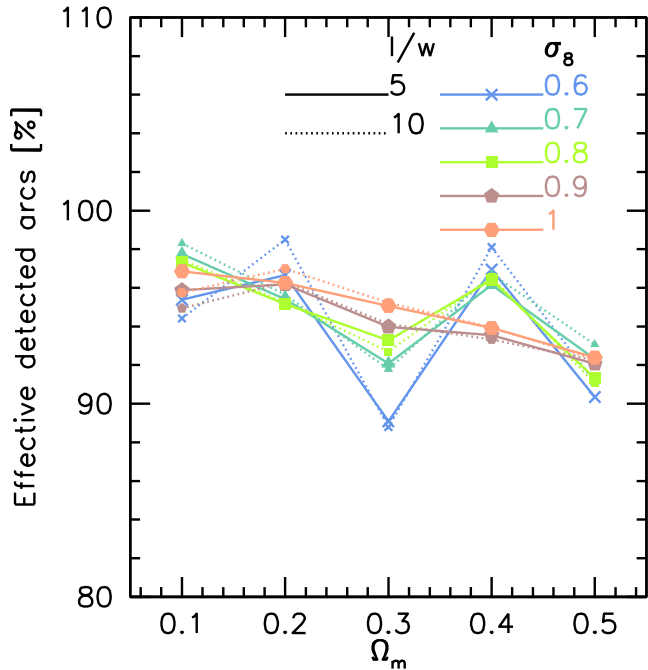


Figure 10. Percentage of arcs effectively detected by considering only lenses having a mass larger than the *Euclid* cluster photometric selection function. Different colour refer to different values of σ_8 , as labelled; solid and dotted lines are for arcs with $l/w \geq 5$ and 10.

galaxy clusters: (i) from photometric data, (ii) from spectroscopic data and (iii) from cosmic shear maps. As shown in ?, the one based on photometric data (see, for example, Bellagamba et al. 2011, and references therein) is expected to be largely the most efficient one. In this case, the minimum mass of galaxy clusters having a number of members larger than three times the rms of the field galaxy counts is expected to be between $5 \times 10^{13} M_{\odot} h^{-1}$ and $8 \times 10^{13} M_{\odot} h^{-1}$ in the redshift range here considered (?). Compared to the minimum mass needed to produce critical lines for sources located at redshift $z_s = 2$ (see Fig. 5), the *Euclid* cluster selection is then slightly higher on a limited redshift range only, namely between $z = 0.2$ and $z = 0.5$. This means that limiting the search for arcs to frames where galaxy clusters have been already identified is expected to not reduce dramatically the number of detected arcs. This is confirmed in Fig. 10, where we show the fraction of arcs that can be effectively detected following this strategy. Same colours indicate same values of σ_8 , as labelled in the figure, while solid and dotted lines refer to arcs with $l/w \geq 5$ and 10, respectively. For the cosmological models here considered, the reduction varies between 2 and 10 per cent and is almost independent of l/w . For the reference *WMAP7* model, the percentage of effectively detected arcs remains about 95 per cent.

In Fig. 11, we show the relative differences in the arc counts between each cosmological model and the reference *WMAP7* cosmology, considering only arcs produced by galaxy clusters above the *Euclid* photometric selection function. In the figure, the colour scale is identical to that adopted in the upper panel of Fig. 4. The white crosses represent the degeneracy curve we found considering the total number of arcs, i.e. without applying the cluster selection function. Although similar, the curve changes in a non-negligible way, especially considering extreme values of the parameters. This underlines the importance of taking into account every kind of selection function when combining theory and observations in arc statistic studies, avoiding possible systematics.

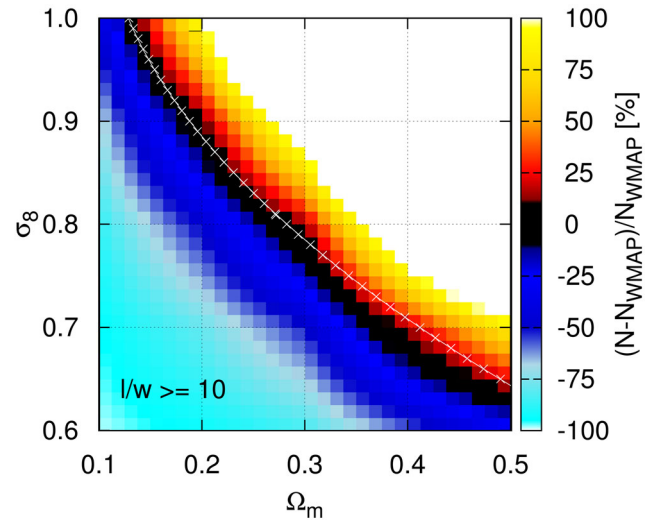


Figure 11. As the upper plot of Fig. 4, but for arcs produced by lenses having a mass larger than the *Euclid* cluster photometric selection function (Sartoris B. et al. 2015). The crossed line represents the degeneracy curve obtained when no selection function is applied.

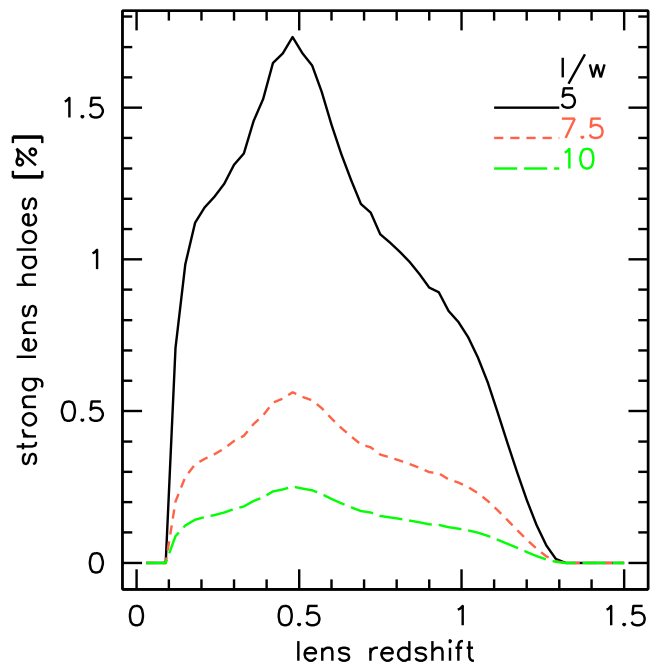


Figure 12. Fraction of galaxy clusters having a mass larger than the *Euclid* cluster photometric selection function producing at least one giant arc. Results are shown for the reference *WMAP7* model. Different line styles refer to different length-to-width ratios, as labelled.

The presence of strong lensing features like arcs can represent a complementary way to confirm the presence of a galaxy cluster. Moreover arcs can be used to improve the estimates of the mass of galaxy clusters, a fundamental ingredient to fully exploit the evolution of their abundance as cosmological probe. For this reason it is important to compute what is the fraction of the galaxy clusters identified in the *Euclid* photometric survey, which are able to produce at least one giant arc. The result for the reference *WMAP7* cosmology as a function of redshift is shown in Fig. 12 for arcs with

$l/w \geq 5, 7.5$ and 10 (black solid, red dashed and green long-dashed lines, respectively). Typical mean values are around 1, 0.33 and 0.15 per cent for $l/w \geq 5, 7.5$ and 10 , respectively. From the figure we notice that the strong lens fraction peaks around $z = 0.5$: this behaviour is a combined effect between the well of the photometric selection function around redshift $z = 0.75$ and the peak – around the same redshifts – of the strong lens counts. Interestingly, for redshift $z \geq 1.3$, the percentage tends to vanish. Finally, we notice that the fact that the strong lensing selection function can be smaller than the photometric cluster one would allow in principle to add extra objects to the *Euclid* cluster sample by looking for strong lensing features only. However, this would require to run the algorithms for arc detection blindly in different areas of the survey. Considering the reference *WMAP7* model and arcs with $l/w \geq 5$, the gain would correspond to approximately 300 extra objects only, all having a relatively low redshift ($0.2 \leq z \leq 0.5$).

Therefore, we can conclude that arc statistics represents a complementary tool to identify galaxy clusters or eventually to prove their presence. In particular, arcs with a small l/w ratio are the best tracers, since they are more numerous, but, at the same time, they are the more difficult to identify because of their similarity with non-lensed galaxies. Finally, our results underline that the codes for arc identification can be run on single frames where galaxy clusters have been already detected with no consequences on the cosmological predictive power of arc statistics.

5 A TEST-BED FOR THE METHOD: THE CLASH SURVEY

While this paper focuses on the sensitivity of arc statistics to cosmological parameters like Ω_m and σ_8 , it is worth mentioning that another paper has been recently submitted by our collaborators Xu et al. (2016) to compare theoretical predictions of arc abundances in a Λ CDM cosmological model and observations. More precisely, in this other work *MOKA* has been used to build up haloes reproducing the properties of the X-ray selected galaxy clusters belonging to the CLASH sample (Postman et al. 2012). Numerical hydrodynamical simulations tailored to reproduce the CLASH selection function (Meneghetti et al. 2014) are also used to derive theoretical predictions. Thus, the work of Xu et al. (2016) provides the best opportunity for validating our methodology against more complex models of the cluster mass distribution and against observed clusters with a known selection function.

The results of this study show that there is an excellent agreement between expectations based on *MOKA* haloes and numerical simulations and the arc counts in the CLASH clusters. More specifically, the lensing efficiency measured in the CLASH sample is 4 ± 1 arcs (with $l > 6$ arcsec and $l/w > 7$) per cluster. *MOKA* simulations return exactly the same number (4 ± 1), while numerical simulations give 3 ± 1 arcs per cluster. Therefore, according to Xu et al. (2016), in terms of efficiency to produce long and thin arcs, observations and simulations based on *MOKA* and numerical hydrodynamical techniques come into full agreement. It is particularly significant that the methodology we have developed for modelling cluster lenses for arc-statistics calculations is fully capturing the complexity of numerically simulated haloes, as evinced from the fact that the cross-sections for giant arcs of *MOKA* generated haloes are well matching those of the haloes described in Meneghetti et al. (2014).

6 CONCLUSIONS

In this work, we have investigated how the number of gravitational arcs depends on cosmology, focusing our attention on the (total) matter density parameter Ω_m and on the initial normalization power spectrum parameter σ_8 . In more detail, we have considered the ranges $\Omega_m = [0.1-0.5]$ and $\sigma_8 = [0.6-1.0]$. Our main results can be summarized as follows.

(i) We confirm that arc statistics is very sensitive to the couple of parameters $\Omega_m-\sigma_8$. In particular, we find that the expected number of arcs is an increasing function of both parameters: this is mostly due to the fact that increasing these parameters boosts the number of lenses.

(ii) The efficiency in producing arcs in cosmologies with high values of σ_8 is larger, since it has an effect also on the structure formation time, that in turn affects some lens structural properties (mainly concentration and triaxiality) relevant for strong lensing.

(iii) A strong degeneracy exists between the two considered cosmological parameters for the number of arcs N_{arcs} ; for the reference *WMAP7* model this is expressed by the relation (2), that is similar, but not equal, in shape to the degeneracy derived from galaxy cluster counts (see equation 3). The differences between the two arise from the non-negligible contribution to $\sigma_{l/w}$ given by the lens structural properties – triaxiality, asymmetries, concentration, substructures and the BCG – and the lensing distance relation.

(iv) Arcs with small l/w ratio are more suitable to constrain cosmological parameters, since they are more numerous. On the other hand, they could be more difficultly identified in the surveys because of their similarity with non-lensed galaxies. We find that if the survey area is sufficiently larger (more than 10 per cent of the full sky) the error budget is dominated by cosmic variance, and the constraining power of arc counts becomes almost independent of the value of l/w . In particular, a survey covering $15\,000\text{ deg}^2$ will be able to distinguish at more than 5σ level the two cosmological models supported by *WMAP7* and *Planck* cosmic microwave background data.

(v) Considering future wide surveys, like the ESA *Euclid* mission, we find that searching for arcs only in frames where galaxy clusters have been previously detected will produce a loss of 2–10 per cent of arcs only (depending on the cosmological model) and a consequent limited degradation of the constraining power of arc counts. This suggests that it will be not necessary to run the computationally expensive algorithms for arc detection on whole wide surveys.

In this paper, we have discussed the potentiality and the capability of the giant arc statistic to constrain the matter density and the initial power spectrum normalization parameter in light of the large data sets that will become available from future wide-field surveys.

ACKNOWLEDGEMENTS

We thank Barbara Sartoris, Cosimo Fedeli and Peter Schneider for useful discussions on the *Euclid* cluster selection function. CG's research is part of the project GLENCO, funded under the European Seventh Framework Programme, Ideas, Grant Agreement no. 259349. CG thanks CNES for financial support. MM and LM acknowledge financial contributions from contracts ASI/INAF/I/023/12/0, by the PRIN MIUR 2010–2011 ‘The dark Universe and the cosmic evolution of baryons: from current surveys to *Euclid*’ and by the PRIN INAF 2012. We acknowledge

support from PRIN-INAF 2014 1.05.01.94.02. We are grateful to the referee Prasenjit Saha for his useful comments.

REFERENCES

- Allen S. W., Schmidt R. W., Fabian A. C., Ebeling H., 2003, *MNRAS*, 342, 287
- Allen S. W., Evrard A. E., Mantz A. B., 2011, *ARA&A*, 49, 409
- Bartelmann M., Schneider P., 2001, *Phys. Rep.*, 340, 291
- Bartelmann M., Huss A., Colberg J. M., Jenkins A., Pearce F. R., 1998, *A&A*, 330, 1
- Bellagamba F., Maturi M., Hamana T., Meneghetti M., Miyazaki S., Moscardini L., 2011, *MNRAS*, 413, 1145
- Benson B. A. et al., 2013, *ApJ*, 763, 147
- Boldrin M., Giocoli C., Meneghetti M., Moscardini L., 2012, *MNRAS*, 427, 3134
- Bonamico M., Despali G., Limousin M., Angulo R., Giocoli C., Soucail G., 2015, *MNRAS*, 449, 3171
- Borgani S. et al., 2001, *ApJ*, 561, 13
- Clowe D., Bradač M., Gonzalez A. H., Markevitch M., Randall S. W., Jones C., Zaritsky D., 2006, *ApJ*, 648, L109
- de Jong J. T. A., Verdoes Kleijn G. A., Kuijken K. H., Valentijn E. A., 2013, *Exp. Astron.*, 35, 25
- Despali G., Giocoli C., Tormen G., 2014, *MNRAS*, 443, 3208
- Eke V. R., Cole S., Frenk C. S., Patrick Henry J., 1998, *MNRAS*, 298, 1145
- Fedeli C., Meneghetti M., Bartelmann M., Dolag K., Moscardini L., 2006, *A&A*, 447, 419
- Gao L., White S. D. M., Jenkins A., Stoehr F., Springel V., 2004, *MNRAS*, 355, 819
- Giocoli C., Moreno J., Sheth R. K., Tormen G., 2007, *MNRAS*, 376, 977
- Giocoli C., Tormen G., van den Bosch F. C., 2008, *MNRAS*, 386, 2135
- Giocoli C., Meneghetti M., Bartelmann M., Moscardini L., Boldrin M., 2012a, *MNRAS*, 421, 3343
- Giocoli C., Meneghetti M., Ettori S., Moscardini L., 2012b, *MNRAS*, 426, 1558
- Henry J. P., 2004, *ApJ*, 609, 603
- Hernquist L., 1990, *ApJ*, 356, 359
- Jing Y. P., Suto Y., 2002, *ApJ*, 574, 538
- Karaji H., 2009, IAC Talks, Astronomy and Astrophysics Seminars from the Instituto de Astrofísica de Canarias Hyper Suprime-Cam (HSC) project for the SUBARU telescope. p. 146
- Kneib J.-P., Natarajan P., 2011, *A&AR*, 19, 47
- Komatsu E. et al., 2011, *ApJS*, 192, 18
- Laureijs R. et al., 2011, preprint ([arXiv:1110.3193](https://arxiv.org/abs/1110.3193))
- LSST Science Collaboration et al., 2009, preprint ([arXiv:0912.0201](https://arxiv.org/abs/0912.0201))
- Macciò A. V., Dutton A. A., van den Bosch F. C., 2008, *MNRAS*, 391, 1940
- Mantz A., Allen S. W., Rapetti D., Ebeling H., 2010, *MNRAS*, 406, 1759
- Mantz A. B., Allen S. W., Morris R. G., Rapetti D. A., Applegate D. E., Kelly P. L., von der Linden A., Schmidt R. W., 2014, *MNRAS*, 440, 2077
- Meneghetti M., Bartelmann M., Moscardini L., 2003, *MNRAS*, 346, 67
- Meneghetti M., Argazzi R., Pace F., Moscardini L., Dolag K., Bartelmann M., Li G., Oguri M., 2007, *A&A*, 461, 25
- Meneghetti M. et al., 2008, *A&A*, 482, 403
- Meneghetti M., Fedeli C., Pace F., Gottlöber S., Yepes G., 2010, *A&A*, 519, A90
- Meneghetti M., Fedeli C., Zitrin A., Bartelmann M., Broadhurst T., Gottlöber S., Moscardini L., Yepes G., 2011, *A&A*, 530, A17
- Meneghetti M., Bartelmann M., Dahle H., Limousin M., 2013, *Space Sci. Rev.*, 177, 31.
- Meneghetti M. et al., 2014, *ApJ*, 797, 34
- Merten J. et al., 2011, *MNRAS*, 417, 333
- Metcalf R. B., Madau P., 2001, *MNRAS*, 563, 9
- Narayan R., Bartelmann M., 1999, in Dekel A., Ostriker J. P., eds, *Formation of Structure in the Universe Gravitational lensing*. Cambridge Univ. Press, Cambridge, p. 360
- Navarro J. F., Frenk C. S., White S. D. M., 1996, *ApJ*, 462, 563
- Neto A. F. et al., 2007, *MNRAS*, 381, 1450
- Planck Collaboration XVI, 2014a, *A&A*, 571, A16
- Planck Collaboration XX, 2014b, *A&A*, 571, A20
- Postman M. et al., 2012, *ApJS*, 199, 25
- Reiprich T. H., Böhringer H., 2002, *ApJ*, 567, 716
- Roza E. et al., 2010, *ApJ*, 708, 645
- Sartoris B. et al., 2015, preprint ([arXiv:1505.02165](https://arxiv.org/abs/1505.02165))
- Schuecker P., Böhringer H., Collins C. A., Guzzo L., 2003, *A&A*, 398, 867
- Sehgal N. et al., 2011, *ApJ*, 732, 44
- Sheth R. K., Tormen G., 1999, *MNRAS*, 308, 119
- Spergel D. et al., 2013, preprint ([arXiv:1305.5422](https://arxiv.org/abs/1305.5422))
- The Dark Energy Survey Collaboration 2005, preprint ([astro-ph/0510346](https://arxiv.org/abs/astro-ph/0510346))
- Torri E., Meneghetti M., Bartelmann M., Moscardini L., Rasia E., Tormen G., 2004, *MNRAS*, 349, 476
- Vikhlinin A. et al., 2009, *ApJ*, 692, 1060
- Xu B. et al., 2016, *ApJ*, 817, 85
- York D. G. et al., 2000, *AJ*, 120, 1579
- Zhao D. H., Jing Y. P., Mo H. J., Börner G., 2003, *ApJ*, 597, L9

This paper has been typeset from a $\text{\TeX}/\text{\LaTeX}$ file prepared by the author.